Acta Materialia 108 (2016) 271–278

Contents lists available at ScienceDirect

Acta Materialia

journal homepage: www.elsevier.com/locate/actamat

Full length article

Analysis of the grain boundary conductivity of singly and doubly doped CeO_2 thin films at elevated temperature

No Woo Kwak, WooChul Jung*

Department of Materials Science and Engineering, Korea Advanced Institute of Science and Technology (KAIST), 291 Daehak-ro, Yuseong-gu Daejeon, 34141, Republic of Korea

ARTICLE INFO

Article history:
Received 16 January 2016
Received in revised form
12 February 2016
Accepted 13 February 2016

Keywords:
Cerium oxide (CeO_2)
Thin film
Electrical conductivity
Grain boundary
Space-charge

ABSTRACT

Acceptor-doped cerium oxides are a promising solid electrolyte material for solid oxide fuel cells (SOFCs) due to their exceptionally high oxygen ion conductivity. Typical solid electrolytes are polycrystalline with a number of grain boundaries, and it is common for grain boundaries to block the motion of mobile oxygen ions as they migrate from one grain to the next. Accordingly, it is important precisely to measure the grain boundary conductivities of doped cerium oxides, particularly at the temperature of relevance (>500 °C). Here, we undertake a quantitative analysis of the transport properties of singly and doubly doped cerium oxides. So that we may precisely extract the grain boundary contribution out of the total conductivity at an elevated temperature (>500 °C), both epitaxial and polycrystalline thin films of the oxides are grown via pulsed layer deposition (PLD) on two different insulating, single-crystal substrates: $Al_2O_3(0001)$ and $SiO_2(001)$, and these are then characterized by a range of analysis tools, in this case TEM, SEM, XRD, ICP-MS and AFM. These samples with controlled microstructures, in combination with in-plane ionic conductivity measurements by impedance spectroscopy as a function of the thickness, temperature and pO_2, enable us precisely to measure the grain boundary conductivity of the doped ceria at temperatures ranging from 620 to 700 °C. The impact of the number and type of dopants on the transport properties are also explored.

1. Introduction

Cerium-based oxides (ceria) are among the most commonly investigated materials with regard to renewable energy and catalysis [1–7]. Remarkable features of ceria, particularly at elevated temperature, such as exceptional crystallographic stability over a wide range of oxygen activity levels [1], good chemical compatibility with most oxides [2], and favorable catalytic activity toward fuel electro-oxidation [3] make ceria a suitable material for solid oxide fuel cells (SOFCs) [4]. Especially when doped with trivalent elements such as samarium or gadolinium, they have been widely used as a solid electrolyte with exceptional oxygen ion conductivity at intermediate temperatures (500–700 °C) [5].

Recently, several interesting studies using doubly doped ceria have gained considerable attention due to the enhanced ionic conductivity of this material as compared with singly doped ceria. Andersson et al. [8] reported that the optimal balance between repulsive elastic and attractive electronic interactions among trivalent dopants and oxygen vacancies can be obtained, minimizing the defect association energy and thereby maximizing the ionic conductivity when Sm and Nd are doubly doped at equal amounts. Driven by this result, many studies have measured the ionic conductivity levels of $Ce_{1-x}Nd_{x/2}Sm_{x/2}O_{2-x/2-\delta}$ systems [9–13]. Moreover, Kim and Navarotsky [14] recently demonstrated a strong correlation between transport properties and formation enthalpies of a solid solution, suggesting that the association between $V_O^{\cdot\cdot}$ and dopants manifests even at high temperatures (400–650 °C). As of now, however, most relevant studies using doubly doped ceria have focused only on the bulk (grain interior) conductivity, while the impact of grain boundaries on the total transport properties has been ignored. Grain boundaries are generally known to block the motion of mobile oxygen vacancies as they migrate from one grain to the next. Moreover, the activation energy for grain boundary conduction (0.90–1.61 *eV*) [15] of ceria doped with rare earth (<10%) is known to be considerably higher than that of the bulk (0.47–0.74 *eV*) [14,15]. Accordingly, with regard to SOFCs operating at relatively reduced temperature (<700 °C) with nano-crystalline

* Corresponding author.
E-mail address: wcjung@kaist.ac.kr (W. Jung).

http://dx.doi.org/10.1016/j.actamat.2016.02.032
1359-6454/

materials, the contributions of the grain boundaries to the total ohmic resistance levels are critical.

In this regard, we undertook quantitative analyses of the transport properties of both singly and doubly doped CeO_2 with Sm and Nd as an acceptor. The conventional conductivity measurement technique using a symmetric sample with metallic electrodes on both sides of a dense oxide pellet does not allow the precise extraction of the grain boundary contribution out of the total conductivity [15,16], particularly at an elevated temperature (>500 °C), because the characteristic frequencies of the corresponding impedance spectra of the bulk and the grain boundary are generally much higher, beyond the frequency limit of a typical device [16]. To address this issue, thin films of doped ceria were grown via pulsed layer deposition (PLD) on two different insulating single-crystal substrates: Al_2O_3(0001) and SiO_2(001). While the films grown on SiO_2 exhibit a microstructure characterized by columnar grains, the films grown on Al_2O_3 are epitaxial. These films with controlled microstructures, in combination with in-plane ionic conductivity measurements by AC impedance spectroscopy (ACIS) as a function of the film thickness, temperature and pO_2, enables the precise determination of the grain boundary conductivity of doped ceria. We found that the grain and grain boundary conductivities of both singly and doubly doped ceria films are nearly identical within a reasonable amount of experimental error. This stands in contrast to the idea of enhanced ionic conductivity as suggested by Andersson et al. [8]. Furthermore, the obtained values of the specific grain boundary conductivities of doped ceria show deviations of several orders of magnitude from those estimated by extrapolating previously reported conductivities at lower temperatures (<350 °C). To the best of our knowledge, this is *the first* report which directly measures the specific grain boundary conductivities of doubly doped ceria with Sm and Nd at temperatures ranging from 620 to 700 °C.

2. Experimental

2.1. Sample preparation

$Ce_{0.95}(Nd_xSm_{1-x})_{0.05}O_{1.975-\delta}$ (x = 0, 0.5, and 1) thin films were prepared by means of pulsed laser deposition (PLD) from oxide targets of the respective materials. The targets were prepared by a combined EDTA-citrate complexing method. $Ce(NO_3)_3\cdot 6H_2O$ (JUNSEI Japan, 99.99% purity), $Nd(NO_3)_3\cdot 6H_2O$ (Alfa Acer, 99.9% purity), and $Sm(NO_3)_3\cdot 6H_2O$ (Alfa Acer, 99.9% purity) were dissolved into deionized water with chelating agents (EDTA and citric acid), and NH_4OH was added to adjust the pH to 9.5. The resulting mixture was kept at 80 °C under continuous stirring until a gel formed. The gel was then dried and placed in a heating mantle at 450 °C for 3–4 h until it was completely self-burned. The obtained powders were calcined in air at 950 °C for 8 h and isostatically cold-pressed at 200 MPa, followed by sintering under air at 1400 °C for 6 h in order to create PLD targets, with heating and cooling rates of 5 °C/min. Thin films with thicknesses ranging from 50 to 400 nm were prepared via PLD on single-crystalline SiO_2(001) and Al_2O_3(0001) substrates 10 × 10 × 0.5 mm^3 in size (MTI Corporation). A Coherent COMPex Pro 205 KrF excimer laser, emitting at a wavelength of 248 nm, was used for ablation with the deposition parameters of a pulsed laser energy of 300 mJ and a laser repetition rate of 5 Hz. During the ablation process, the substrate temperature and O_2 working pressure were kept at 700 °C and 7.5 mTorr, respectively. After the deposition process, all of the samples were annealed in air in a tube furnace at 700 °C for 2 h to ensure that they were fully oxidized.

2.2. Physical characterization

X-ray diffraction (XRD) measurements were taken of the deposited films on SiO_2(001) substrate using a Bragg-Brentano diffractometer (Rigaku Ultima IV, Tokyo, Japan, Cu-Kα wavelength (λ = 1.541 Å)). For both the in-plane and out-of-plane reflections, high-resolution x-ray diffraction (HR-XRD) measurements were taken of the deposited films, particularly of the Al_2O_3(0001) substrate using a diffractometer (X'Pert-PRO MRD, PANalytical) operated at 45 kV and 40 mA with a fixed Cu anode. A hybrid monochromator, consisting of a four-bounce Ge(220) crystal and a parabolic multilayer mirror, was employed in the incident beam path to provide monochromatic x-rays from the Cu Kα (1.540598 Å) with reproducibility of better than 0.0001 deg. The grain size, morphology, and surface roughness of the thin films were characterized by an atomic force microscope (AFM) analysis using a Bruker (Innova) device in tapping mode. The cross-sections of the resulting films were examined using a (S-4800, Hitachi) scanning electron microscope (SEM), while for the high-resolution imaging, (JEM-3010, JEOL) transmission electron microscopy (TEM) micrographs were used at an acceleration voltage of 300 kV. The chemical composition of the initial powders and the deposited films were measured using an inductively coupled plasma mass spectrometer (ICP-MS, 7700S, Agilent) in the He mode, after dissolution in a (HNO_3: HCl = 7:3) solution at 200 °C for 30 min. The depth profiles of the Si inside the doped CeO_2 films were analyzed by (Cameca IMS 7f) magnetic sector secondary ion mass spectrometry; primary 6 kV Cs^+ ions (9 kV of effective voltage) raster scanned over (130 × 130 μm^2) were used to generate negatively charged secondary ions.

2.3. In-plane conductivity measurement

The in-plane conductivity measurements were carried out using AC impedance spectroscopy (ACIS, VSP-300, Biologic) at frequencies ranging from 2 MHz to 1 Hz. Two platinum electrodes (200 nm in thickness with a distance of 1 mm between the electrodes) were sputtered onto the films using a metal shadow mask, serving as electrodes. An AC amplitude of 100 mV was used after confirming that this voltage lies within the linear regime of the sample's current–voltage response. A tube furnace was used for the measurements at temperatures between 620 °C and 700 °C in oxygen/argon gas mixtures with the corresponding pO_2 values ranging from 10^{-3}–0.21 atm. Each sample was considered to reach equilibrium at a given temperature and oxygen partial pressure, after confirming that the changes in the impedance spectra lie within 2% error between sequential measurements separated in time by 10 min. To eliminate the possibility of additional current conduction through the insulating substrates, their resistance levels without any film were separately measured.

3. Results and discussion

3.1. Physical characterization of the ceria films

The XRD spectra of doped CeO_2 thin films grown on SiO_2(001) and Al_2O_3(0001) single-crystal substrates at 700 °C are shown in Fig. 1. The out-of-plane results (2θ scan) indicate that the films on SiO_2(001) are in the polycrystalline cubic fluorite phase with several orientations of (111), (200), and (311) (Fig. 1a). There is no evidence of amorphous films or diffraction peaks other than those in the cubic fluorite phase. On the other hand, several features indicate that the films on Al_2O_3(0001) are epitaxially grown. For example, the out-of-plane X-ray spectra show only (111) peaks. Furthermore, the number and positions of the diffraction peaks

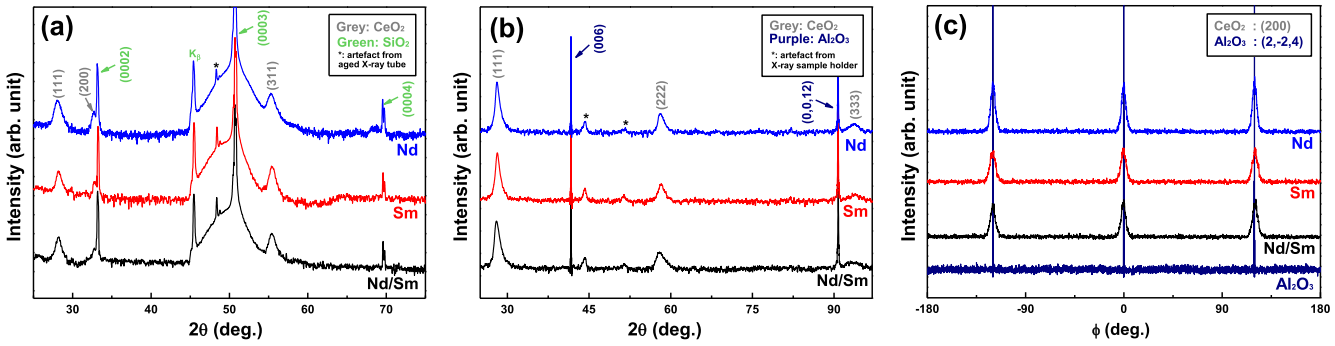

Fig. 1. X-ray diffraction data for the doped CeO_2 thin films with thickness of ~200 nm. Out-of-plane diffraction patterns (2θ scan) (a) on SiO_2(001) substrate and (b) on Al_2O_3(0001) substrate. (c) In-plane diffraction patterns (ϕ scan) comparing the Al_2O_3(2,-2,4) substrate and the CeO_2(200) deposited film.

observed by in-plane XRD (ϕ scan) are consistent, for each film orientation, with the 120° rotational symmetry of the crystallographic plane normal to the incident beam, confirming good alignment registry between the film and the substrate. The epitaxial growth of CeO_2(111) film onto an Al_2O_3(0001) single-crystal substrate was also reported elsewhere, mainly due to the similar unit cells (hexagonal unit cell) of both surfaces [17,18]. In fact, the out-of-plane lattice parameter is independent of the film thickness, particularly for thick films (>58 nm), suggesting that the misfit strain is negligible. However, the thinnest epitaxial film with a thickness of 17 nm is highly compressed in-plane and dilated in a direction normal to the film surface. The calculated values of the in-plane strain of the CeO_2 doped with Nd at 5% (NDC) are shown as a function of the thickness in Fig. S1. There is no distinct difference between the films with three different chemical compositions, *e.g.*, $Ce_{0.95}(Nd_xSm_{1-x})_{0.05}\ O_{1.975-\delta}$ (x = 0, 0.5, and 1).

TEM micrographs of the ceria films grown on different substrates are shown in Fig. 2, displaying a dense film with no visible pores. The microstructure of the films on SiO_2(001) appears to be columnar, with high-aspect-ratio grains extending from the substrate to the surface, while no grain boundaries are observed in the films on Al_2O_3(0001), confirming their epitaxial characteristic. AFM images of the surfaces of the ceria films are shown in Fig. 3. The lateral dimensions all span 1 μm. The vertical dimension in the image is indicated on the z-axis scale as 2 nm. The doped ceria films with thicknesses between 158 and 211 nm deposited at 700 °C onto a SiO_2(001) single-crystal substrate exhibit grain sizes ranging from 60 to 95 nm and RMS surface roughness levels of 0.5 ± 0.2 nm. Such flat and dense layers are not accessible from the oxide pellets used with the conventional bulk ceramic process.

In addition, as shown in Table 1, the chemical compositions of the PLD target materials and the deposited films are investigated via ICP-MS, revealing that these compositions are highly consistent with those in the bulk targets over the entire dopant concentration range. However, the SIMS depth profiling results reveal that both the epitaxial and polycrystalline ceria films contain non-negligible amounts of Si, as shown in Fig 4. Si (or more precisely SiO_x) contamination in ceria is unavoidable because the starting oxide powers used to create ceria PLD targets typically retain a few tens of ppm levels of Si. In fact, it is known that SiO_x easily disperses along the grain boundaries of ceria, blocking oxygen ion migration across these boundaries [19,20]. In this study, we carefully established the temperature and time for the pre-annealing process (700 °C, 2 h) and the impedance measurements (620–700 °C, total 12 h), respectively, so as to prevent further Si contamination, particularly in the polycrystalline films, through Si diffusion from the SiO_2 substrate through the ceria grain boundaries (see Fig. S2).

In sum, the films obtained in this study have several advantages over typical ceramic pellets in terms of controlled microstructures and compositions. They are free of secondary phases, pores or cracks (and even grain boundaries in some films). Consequently, they serve as an appropriate model system for quantitatively analyzing the bulk and grain boundary conductivities of doped CeO_2.

3.2. Impedance spectra of ceria films

Here, the ionic conductivity of the doped CeO_2 was obtained by measuring the resistance of the films with two dense and non-ionically conducting Pt electrodes on the surface. To prevent the current constriction effect, which often occurs during the in-plane conductivity measurements of a thin film with a cell geometry similar to that in this study, the spacing between the Pt electrode was set to 1 mm after comparing it with electrolyte thicknesses

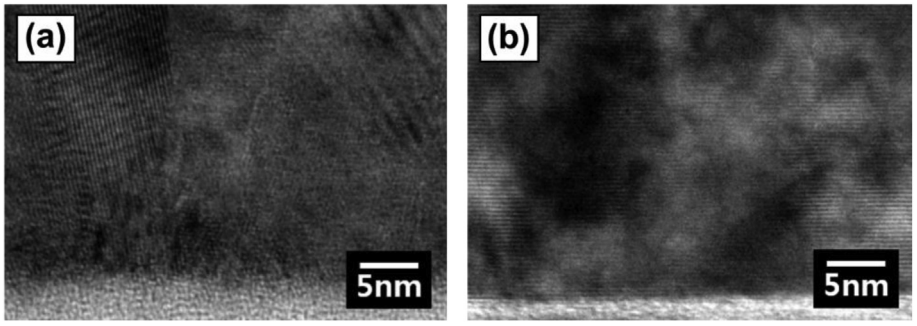

Fig. 2. Transmission electron microscopy micrographs of Nd doped CeO_2 films in the work. (a) Columnar polycrystalline film (thickness: 158 nm) on SiO_2(001) substrate, and (b) epitaxial film (thickness: 167 nm) on Al_2O_3(0001) substrate.

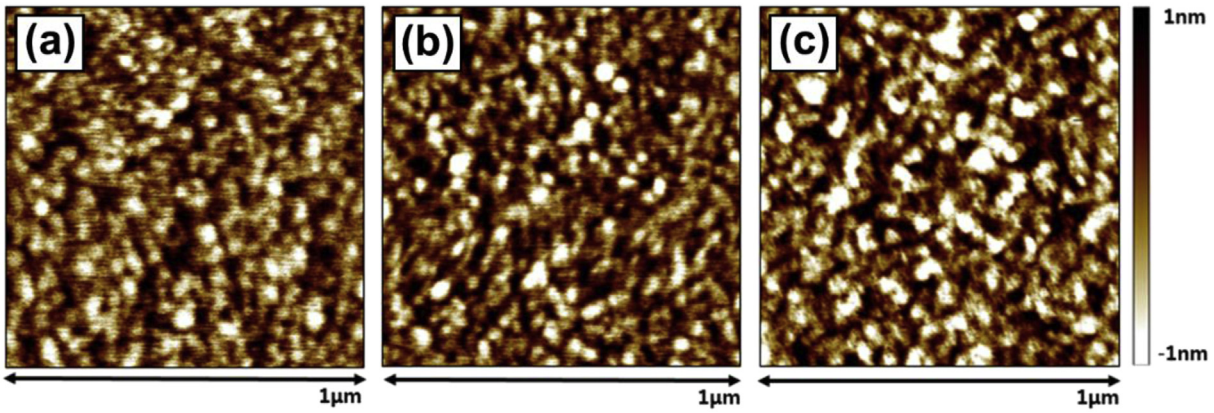

Fig. 3. AFM micrographs of the doped CeO_2 films with thickness of ~200 nm on SiO_2(001) substrates. (a) Nd doped CeO_2 (NDC), (b) Sm doped CeO_2 (SDC), and (c) Nd/Sm doubly doped CeO_2 (SNDC).

Table 1
Detailed physical and chemical parameters of the singly and doubly doped CeO_2 samples. The values of film thickness and grain size were obtained from scanning electron microscopy and atomic force microscope, respectively. The chemical composition of targets and films were analyzed by inductively coupled plasma mass spectrometer.

Sample	Film thickness (nm)		Grain size (nm)		Composition (atomic %)	
	Columnar	Epitaxial	Columnar	Epitaxial	Target	Film
$Ce_{0.95}Nd_{0.05}O_{1.975-\delta}$	158 ± 7	167 ± 20	77.8 ± 5.2	Single crystalline	Ce: 94.9 Nd: 5.1	Ce: 94.9 Nd: 5.1
$Ce_{0.95}Sm_{0.05}O_{1.975-\delta}$	168 ± 14	170 ± 14	77.2 ± 17.8	Single crystalline	Ce: 95.0 Sm: 5.0	Ce: 94.7 Sm: 5.3
$Ce_{0.95}(Nd/Sm)_{0.05}\ O_{1.975-\delta}$	211 ± 47	234 ± 40	77.4 ± 14.0	Single crystalline	Ce: 95.2 Nd: 2.4 Sm: 2.4	Ce: 94.9 Nd: 2.5 Sm: 2.6

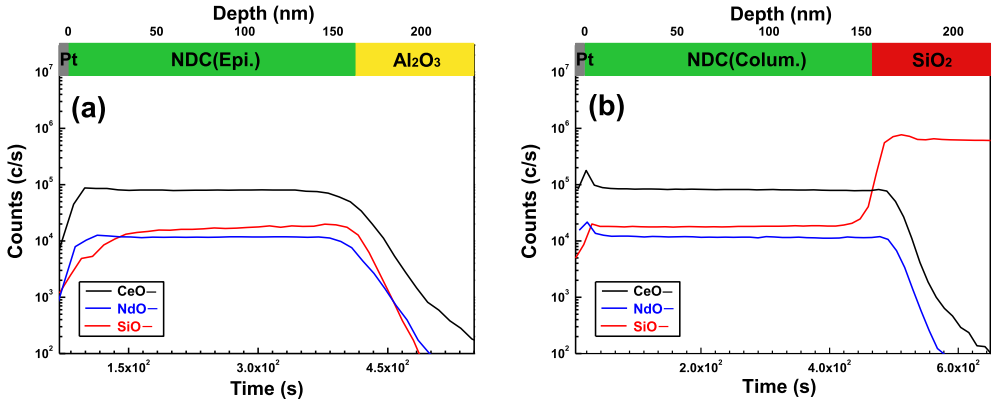

Fig. 4. Depth profiles of Si (red), Ce (black), and Nd (blue), obtained by SIMS analysis after the AC impedance measurements. The substantial amounts of elemental Si are detected both of (a) epitaxial and (b) columnar films. (For interpretation of the references to colour in this figure legend, the reader is referred to the web version of this article).

ranging from several dozen to several hundreds of nm, *e.g.*, 58–376 nm [21]. Differing from the typical impedance spectra of bulk oxide pellets, that include two separate semicircles (*e.g.*, one from the bulk interior and the other from the grain boundary) in the Nyquist plot [16], the corresponding impedance spectra of the films in this work show only one nearly ideal semicircle, even for the polycrystalline films on SiO_2(001) substrates (see Fig. 5). This is attributed to the substrate stray capacitance of ~10^{-10} F, a value which is several orders of magnitude higher than the capacitance levels of the bulk and grain boundary of the films. Given that the bulk and the grain boundary impedance spectra cannot be distinguished, only the sum of both resistive contributions was measured in this study. Accordingly, given its nearly ideal semicircular shape, the single impedance spectra can be modeled by a parallel R–C circuit. More generally, the capacitor is replaced by a constant-phase element (CPE), for which the overall impedance is determined by $Z(\omega) = R[1 + (i\omega)^{\alpha}QR]^{-1}$ $(0.95 \leq \alpha \leq 1)$ (the inert of Fig. 5a). Similar observations have been reported elsewhere [22,23]. In general, the film resistances decrease with the thickness, and columnar films always have greater resistance levels than the epitaxial films at similar thicknesses.

It should be noted that the electronic leakage current through the insulating substrates may not be negligible, especially at higher temperatures [24–27]. In order to eliminate such a possibility, the resistances of bare substrates were separately measured, revealing that they are always greater than one order of magnitude higher than those of the thinnest ceria film (Fig. S3). Furthermore, the resistance of all samples remains constant as a function of the oxygen partial pressure, ranging from 10^{-3}–0.21 atm, clearly confirming that it is oxygen ion conduction through the films (Fig. 5b).

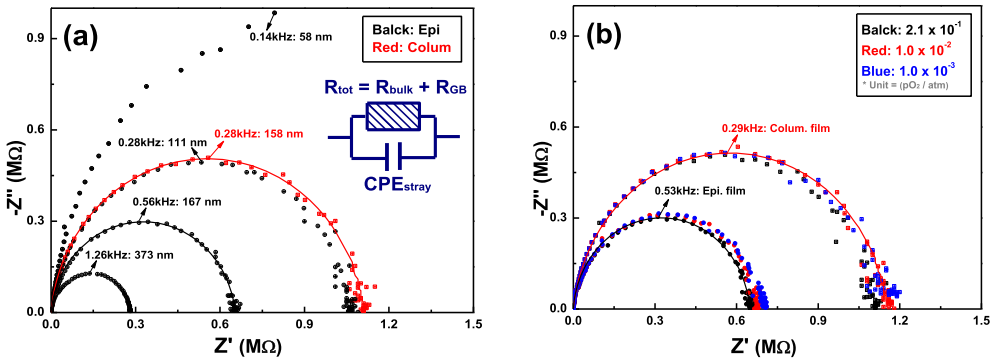

Fig. 5. Typical impedance spectra of columnar (square) and epitaxial (sphere) NDC films at 700 °C (a) with different film morphology and thickness (at $pO_2 = 0.21$ atm), and (b) with different pO_2 values ranging from 0.21 to 10^{-3} atm (at thickness of 170 nm). The fitting results (solid line) modelled with the equivalent circuit (inset in Fig. 5a) of deposited ceria films and the values of peak frequencies of the semicircles are included in the figures.

Because the origin of the impedance spectra is understood, the total conductivity of the doped ceria films is calculated as

$$\sigma_{tot}^{ion} = \frac{1}{R_{film}}\left(\frac{L}{A}\right) \quad (1)$$

in which L and A are the current conducting length and area, respectively.

Fig. 6 shows the total conductivity of the epitaxial NDC films as a function of the film thickness. The conductivity decreases slightly as the thickness decreases, particularly for thinner films (<58 nm). The reason for this trend is not obvious, but similar observations have been reported and explained in terms of film–substrate interface effects in conjunction with the space-charge [28,29] or inherent film strain [30–32]. Considering the relatively large acceptor dopant concentration, *e.g.*, 5%, the former seems unlikely to be the case in this study. Therefore, the compressive in-plane strain from the lattice mismatch between the film and the substrate likely caused the decrease in the total conductivity of the thinner films (<58 nm). Schichtel and Janek et al. [31] also reported that compressed film toward the in-plane direction decreased the ionic conductivity of certain oxide thin films, such as Y-stabilized ZrO_2 and Sc_2O_3 multilayers, mainly due to the presence of negative nominal misfits at the interfaces between the films. This contention is further supported by the XRD results, showing that thinner films have non-negligible degrees of in-plane strain (see Fig. S1). However, a detailed interpretation of the film strain effects is outside the scope of this work. Here, in order to eliminate such interfacial effects and thereby to determine the precise bulk conductivity of the doped epitaxial ceria films, the conductivity was measured only with films that are thicker than 170 nm.

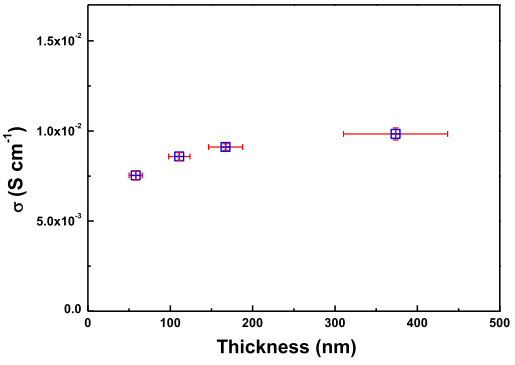

Fig. 6. Ionic conductivity of epitaxial NDC films as a function of thickness. The conductivity decreases slightly as the thickness decreases, particularly for thinner films (<58 nm). Error bars corresponding to the standard deviation of data are shown.

3.3. Specific grain boundary conductivity

In Fig. 7a, the conductivities of the epitaxial films with thicknesses between 170 and 234 nm are shown as a function of the temperature. Given that there is no grain boundary in the epitaxial film, these oxygen ion conductivity values are equal to those of the bulk (or grain interior). The bulk conductivities show values comparable within an experimental error range regardless of the different numbers and/or types of dopants. The activation energy E_a, which is associated with oxygen migration, considering that the oxygen vacancy concentration is fixed by the amount of dopants, is 0.74 ± 0.01 *eV* for all compositions, equivalent to the value in a previous investigation of single-crystal ceria films on Al_2O_3(0001) substrates [33]. There is no significant enhancement of the oxygen conductivity of the doubly doped ceria, as expected from the DFT simulation results [8]. With regard to the columnar films (Fig. 7b), the values of the conductivity decrease by nearly a factor of 2 when compared with those in epitaxial films. Furthermore, the polycrystalline films show higher activation energy levels of 0.96, 0.97, and 0.90 *eV* for the Nd, Sm, and Nd/Sm doped films, respectively. The decreased conductivity and increased *Ea* values of the columnar films are attributed to the existence of grain boundaries aligned perpendicularly to the film surface. Again, the difference of the conductivities between the singly and doubly doped polycrystalline films is not conspicuous.

The main goal of this work is to obtain specific grain boundary conductivities at an elevated temperature (>500 °C). The specific grain boundary conductivity is a microstructure-independent property which is normalized by the total length of the grain boundaries, as shown below using a brick-layer model [34,35].

$$\sigma_{GB}^{spec} = \frac{1}{R_{GB}}\left(\frac{L}{A}\right)\frac{\delta_{GB}}{d} \quad (2)$$

Here, δ_{GB} is the grain boundary width and d is the lateral grain size.

In this study, in order to obtain the grain boundary width, δ_{GB}, of the ceria films effectively, the values of the space-charge potential at the grain boundaries were estimated using the method demonstrated by Maier et al. in [23]. It is well known that the grain boundary core of acceptor-doped CeO_2 is inherently positively charged, which in turn is macroscopically balanced by an oxygen-vacancy-depleted space-charge region to maintain global electroneutrality [19,36]. The width of the corresponding space-charge

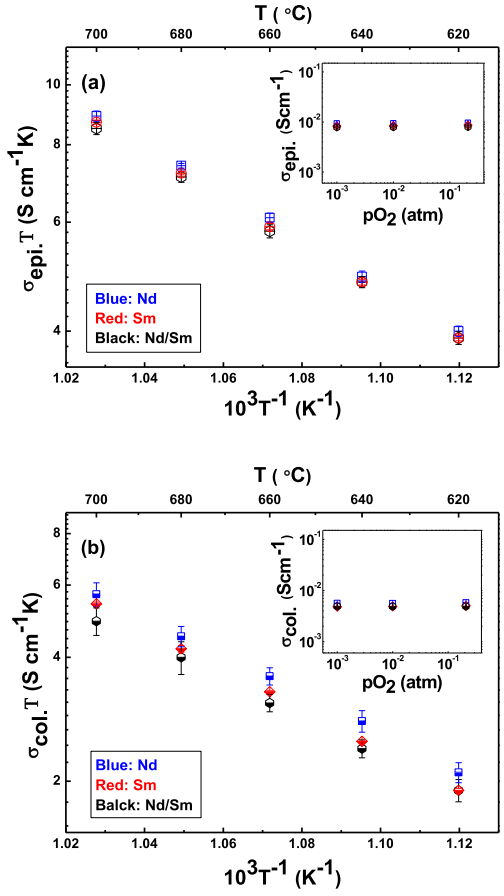

Fig. 7. Arrhenius plot of the electrical conductivity of singly and doubly doped CeO_2 films: (a) on Al_2O_3(0001) substrate, and (b) SiO_2(001) substrate. Double-logarithmic plots (insets) for (a) epitaxial and (b) columnar films of the electrical conductivity vs. pO_2 at 700 °C show the electrical conductivity is fully ionic. For both (a) and (b), error bars corresponding to the standard deviation of data are shown, and may appear smaller than data points.

region, which varies with the potential resulting from the positive charge at the grain boundary core, can be assumed to be half of δ_{GB}. Under a Mott-Schottky approximation condition, the relationship between the effective grain boundary width and the space-charge potential is shown below.

$$\delta_{GB} = 2\lambda^* = 2\sqrt{\frac{\varepsilon_0\varepsilon_r}{e[V_O^{\cdot\cdot}]}*\Delta\Phi(o)} \quad (3)$$

In this equation, $\Delta\Phi(o)$ is the space-charge potential at the grain boundary; $[V_O^{\cdot}]$ is the oxygen vacancy concentration, which is half of the dopant concentration; and ε_0 and ε_r are the vacuum permittivity and the dielectric constant, respectively.

The space-charge potential, $\Delta\Phi(o)$, can also be determined from the ratio of the resistivity of the specific grain boundary and the bulk, as reported by Guo and Maier [20]:

$$\frac{\rho_{GB}}{\rho_{bulk}} = \frac{\exp(2e\Delta\Phi(o)/kT)}{4e\Delta\Phi(o)/kT} \quad (4)$$

Under the assumption of an unvarying dielectric constant of 30 between the bulk and the grain boundary of ceria [37,38], equation (4) can also be expressed as a function of measurable parameters ($R_{epi.}$, $R_{col.}$, and d) as well as δ_{GB} (see equation (3)).

$$\frac{\rho_{GB}}{\rho_{bulk}} = \frac{R_{GB}}{R_{bulk}}*\frac{C_{GB}}{C_{bulk}} \approx \frac{R_{col.} - R_{epi.}}{R_{epi.}}*\frac{d}{2\lambda^*} \quad (5)$$

By solving equations (2)–(5), it becomes possible to determine values of $\Delta\Phi(o)$ of 0.26–0.27 *V* for each of the films, as shown in Fig. 8a. Also, the grain boundary width of approximately 1.10 nm as calculated from $\Delta\Phi(o)$ allows the extraction of the specific grain boundary conductivity at an elevated temperature (Fig. 8b). In Table 2, the values of the conductivity and E_a for different chemical compositions of $Ce_{1-x}Nd_{x/2}Sm_{x/2}O_{2-x/2-\delta}$ are shown. Not only the bulk, but also the grain boundaries manifest analogous properties in spite of the different types and numbers of dopants used. While there have been many research efforts directed towards confirming the enhanced ionic conductivity of $Ce_{1-x}Nd_{x/2}Sm_{x/2}O_{2-x/2-\delta}$ systems, they remain unsatisfactory and their conclusions are controversial [9–13]. This has been due to the morphological and chemical complexity of the typical ceramic pellets used. Gao et al. [39] also reported that different synthesis routes result in wholly changed ionic conductivity values of doubly doped ceria oxide pellets, even with the same chemical compositions. Here, we carefully control both the microstructure and chemical composition using dense thin films which are free of secondary phases, pores or cracks. Again, a significant enhancement in the bulk and grain boundary

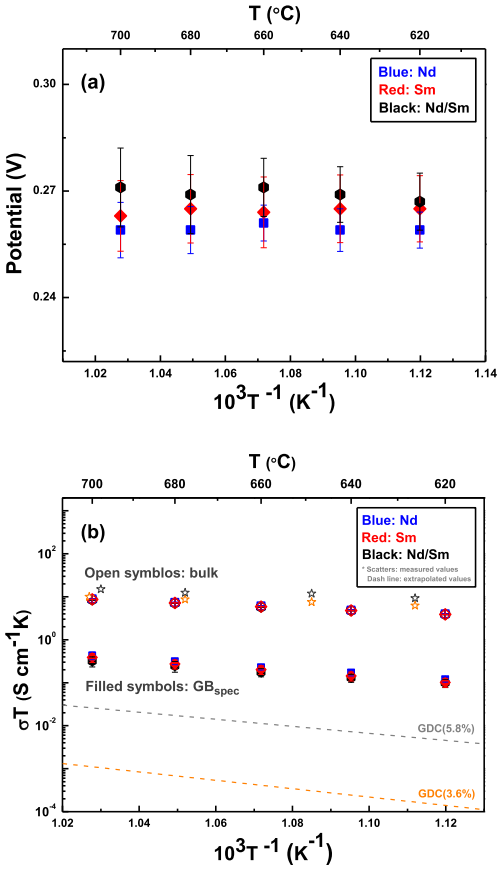

Fig. 8. (a) The space-charge potentials at the grain boundary of the doped CeO_2 films. (b) The values of bulk (open symbols) and a specific grain boundary (filled symbols) conductivities of doped CeO_2 (pO_2 = 0.21 atm). Blue, red and black dots indicate the films in this work with a dopant of Nd, Sm and Nd/Sm, respectively. For both (a) and (b), error bars corresponding to the standard deviation of data are shown, and may appear smaller than data points. Grey and orange dots indicate the values of reported conductivities of 5.8% and 3.6% Gd doped CeO_2 from Ref. [15]. (For interpretation of the references to colour in this figure legend, the reader is referred to the web version of this article).

Table 2
The values of Activation energies and conductivities of the doped CeO_2 films in the work. Both values were obtained under pO_2 of 0.21 atm at 620 °C.

Sample	*Ea* (*eV*)		σ (S/cm)	
	Bulk	$GB_{spec.}$	Bulk	$GB_{spec.}$
NDC	0.74	1.17	4.50×10^{-3}	1.35×10^{-4}
SDC	0.75	1.23	4.36×10^{-3}	1.14×10^{-4}
SNDC	0.73	1.10	4.39×10^{-3}	1.11×10^{-4}

transport properties was not observed.

On the other hand, the obtained values of the specific grain boundary conductivities of doped ceria show deviations of several orders of magnitude from those estimated by extrapolating the reported conductivities at a lower temperature (<350 °C) using ceramic pellets. For example, the specific grain boundary conductivity levels of $Ce_{0.95}Nd_{0.05}O_{1.975-\delta}$ at temperatures ranging from 620 to 700 °C are greater by one order and three orders of magnitude when compared with the estimated values of $Ce_{0.942}Gd_{0.058}O_{1.971-\delta}$ and $Ce_{0.964}Gd_{0.036}O_{1.982-\delta}$, respectively [15] (see Fig. 8b). This is also the case even though the bulk conductivities are nearly identical (within 80% error) to the values reported in the same work. It is clear that extrapolation with temperature exceeding 300 °C cannot guarantee reasonable reliability when attempting to determine the specific grain boundary conductivities. In fact, $\Delta\Phi(o)$ is known to decrease with the temperature, ensuring an increase in the specific grain boundary conductivity with the temperature [40]. This may be another reasons behind such large inconsistencies in terms of the specific grain boundary conductivity at elevated temperatures. This contention also further supported by the fact that our calculated values of $\Delta\Phi(o)$ (0.26–0.27 *V*) at 620–700 °C are lower than those obtained at 350 °C (*e.g.*, 0.36 *V* for $Ce_{0.942}Gd_{0.058}O_{1.971-\delta}$ and 0.46 *V* for $Ce_{0.964}Gd_{0.036}O_{1.982-\delta}$). These observations clearly demonstrate the need for directly measurements of the interface transport properties of electrolyte materials at the temperatures of relevance.

4. Conclusions

Both epitaxial and columnar polycrystalline thin films of singly and doubly doped cerium oxides were successfully grown via pulsed layer deposition (PLD) on two different insulating, single-crystal substrates: $Al_2O_3(0001)$ and $SiO_2(001)$. This, in combination with the in-plane ionic conductivity measurements by ACIS, enables one to obtain the values of both the bulk and the specific grain boundary conductivities of doped ceria films directly, particularly at elevated temperatures ranging from 620 to 700 °C, the SOFC operation temperature range. Enhanced ionic transport properties by the double-dopant effects of Sm and Nd were not observed in this study, in contrast to the suggestion by Andersson et al. in [8]. However, the values of the specific grain boundary conductivities of the doped ceria systems as determined here show deviations of several orders of magnitude from those estimated by previously reported conductivities extrapolating at lower temperatures (<350 °C), indicating the importance of directly measuring the grain boundary conductivities of electrolyte materials at elevated temperatures. The methodology suggested in this study can be used for investigating the interface transport properties of many other conducting materials under their relevant operating conditions.

Acknowledgements

This work was supported by the Korea CCS R&D Center (KCRC) grant funded by the Korea government (Ministry of Science, ICT & Future Planning) (2014M1A8A1049350). Additional support was provided by the Basic Science Research Program through the National Research Foundation of Korea (NRF) funded by the Ministry of Science, ICT & Future Planning (NRF-2014R1A1A1003008) and by the In-house Research and Development Program of the Korea Institute of Energy Research (KIER) (B3-2411).

Appendix A. Supplementary data

Supplementary data related to this article can be found at http://dx.doi.org/10.1016/j.actamat.2016.02.032.

References

[1] A. Atkinson, S. Barnett, R.J. Gorte, J.T.S. Irvine, A.J. McEvoy, M. Mogensen, S.C. Singhal, J. Vohs, Advanced anodes for high-temperature fuel cells, Nat. Mater 3 (2004) 17–27.
[2] J.W. Fergus, Electrolytes for solid oxide fuel cells, J. Power Sources 162 (2006) 30–40.
[3] W.C. Chueh, Y. Hao, W. Jung, S.M. Haile, High electrochemical activity of the oxide phase in model ceria–Pt and ceria–Ni composite anodes, Nat. Mater 11 (2012) 155–161.
[4] V.V. Kharton, F.M. Figueiredo, L. Navarro, E.N. Naumovich, A.V. Kovalevsky, A.A. Yaremchenko, A.P. Viskup, A. Carneiro, F.M.B. Marques, J.R. Frade, Ceria-based materials for solid oxide fuel cells, J. Mater. Sci. 36 (2001) 1105–1117.
[5] E.D. Wachsman, K.T. Lee, Lowering the temperature of solid oxide fuel cells, Science 334 (2011) 935–939.
[6] W.C. Chueh, C. Falter, M. Abbott, D. Scipio, P. Furler, S.M. Haile, A. Steinfeld, High-flux solar-driven thermochemical dissociation of CO_2 and H_2O using nonstoichiometric ceria, Science 330 (2010) 1797–1801.
[7] J.A. Rodriguez, S. Ma, P. Liu, J. Hrbek, J. Evans, M. Perez, Activity of CeO_x and TiO_x nanoparticles grown on Au(111) in the water-gas shift reaction, Science 318 (2007) 1757–1760.
[8] D.A. Andersson, S.I. Simak, N.V. Skorodumova, I.A. Abrikosov, B. Johansson, Optimization of ionic conductivity in doped ceria, Proc. Natl. Acad. Sci. U.S.A. 103 (2006) 3518–3521.
[9] S. Omar, E.D. Wachsman, J.C. Nino, Higher ionic conductive ceria-based electrolytes for solid oxide fuel cells, Appl. Phys. Lett. 91 (2007) 144106.
[10] S. Omar, E.D. Wachsman, J.C. Nino, Higher conductivity Sm^{3+} and Nd^{3+} co-doped ceria-based electrolyte materials, Solid State Ion. 178 (2008) 1890–1897.
[11] B. Li, Y. Liu, X. Wei, W. Pan, Electrical properties of ceria Co-doped with Sm^{3+} and Nd^{3+}, J. Power Sources 195 (2010) 969–976.
[12] R.M. Kasse, J.C. Nino, Ionic conductivity of $Sm_xNd_yCe_{0.9}O_{2-\delta}$ codoped ceria electrolytes, J. Alloys. Comp. 575 (2013) 399–402.
[13] A. Rai, P. Mehta, S. Omar, Ionic conduction behavior in $Sm_xNd_{0.15-x}Ce_{0.85}O_{2-\delta}$, Solid State Ion. 263 (2014) 190–196.
[14] S. Buyukkilic, S. Kim, A. Navrotsky, Defect chemistry of singly and doubly doped ceria: correlation between ion transport and energetics, Angew. Chem. 53 (2014) 9517–9521.
[15] H.J. Avila-Paredes, K. Choi, C.-T. Chen, S. Kim, Dopant-concentration dependence of grain-boundary conductivity in ceria: a space-charge analysis, J. Mater. Chem. 19 (2009) 4837.
[16] E.C.C. Souza, W.C. Chueh, W. Jung, E.N.S. Muccillo, S.M. Haile, Ionic and electronic conductivity of nanostructured, samaria-doped ceria, J. Electrochem. Soc. 159 (2012) K127–K135.
[17] S.V.N.T. Kuchibhatla, P. Nachimuthu, F. Gao, W. Jiang, V. Shutthanandan, M.H. Engelhard, S. Seal, S. Thevuthasan, Growth-rate induced epitaxial orientation of CeO_2 on $Al_2O_3(0001)$, Appl. Phys. Lett. 94 (2009) 204101.
[18] M.I. Nandasiri, P. Nachimuthu, T. Varga, V. Shutthanandan, W. Jiang, S.V.N.T. Kuchibhatla, S. Thevuthasan, S. Seal, A. Kayani, Influence of growth rate on the epitaxial orientation and crystalline quality of CeO_2 thin films grown on Al_2O_3 (0001), J. Appl. Phys. 109 (2011) 013525.
[19] X. Guo, W. Sigle, J. Maier, Blocking grain boundaries in yttria-doped and undoped ceria ceramics of high purity, J. Am. Ceram. Soc. 86 (2003) 77–87.
[20] X. Guo, J. Maier, Grain boundary blocking effect in zirconia: a schottky barrier analysis, J. Electrochem. Soc. 148 (2001) E121–E126.
[21] J.L. Hertz, H.L. Tuller, Measurement and finite element modeling of triple phase boundary-related current constriction in YSZ, Solid State Ion. 178 (2007) 915–923.
[22] M.C. Gobel, G. Gregori, X. Guo, J. Maier, Boundary effects on the electrical conductivity of pure and doped cerium oxide thin film, Phys. Chem. Chem. Phys. 12 (2010) 14351–14361.
[23] M.C. Gobel, G. Gregori, J. Maier, Mixed conductivity in nanocrystalline highly acceptor doped cerium oxide thin films under oxidizing conditions, Phys. Chem. Chem. Phys. 13 (2011) 10940–10945.
[24] H.R. Kim, J.C. Kim, K.R. Lee, H.I. Ji, H.W. Lee, J.H. Lee, J.W. Son, 'Illusional' nano-size effect due to artifacts of in-plane conductivity measurements of ultra-thin film, Phys. Chem. Chem. Phys. 13 (2011) 6133–6137.

[25] S.M. Kim, J.-W. Son, K.-R. Lee, H. Kim, H.-R. Kim, H.-W. Lee, J.-H. Lee, Substrate effect on the electrical properties of sputtered YSZ thin films for co-planar SOFC applications, J. Electroceram 24 (2010) 153–160.
[26] F.G. Will, H.G. Delorenzi, K.H. Janora, Conduction mechanism of single-crystal alumina, J. Am. Ceram. Soc. 75 (1992) 295–304.
[27] H. Jain, A.S. Nowick, Electrical-conductivity of synthetic and natural quartz crystals, J. Appl. Phys. 53 (1982) 477–484.
[28] J. Maier, Ionic conduction in space charge regions, Prog. Solid State Chem. 23 (1995) 171–263.
[29] X. Guo, J. Maier, Ionically conducting two-dimensional heterostructures, Adv. Mater 21 (2009) 2619–2631.
[30] N. Schichtel, C. Korte, D. Hesse, J. Janek, Elastic strain at interfaces and its influence on ionic conductivity in nanoscaled solid electrolyte thin films—-theoretical considerations and experimental studies, Phys. Chem. Chem. Phys. 11 (2009) 3043–3048.
[31] N. Schichtel, C. Korte, D. Hesse, N. Zakharov, B. Butz, D. Gerthsen, J. Janek, On the influence of strain on ion transport: microstructure and ionic conductivity of nanoscale YSZ|Sc_2O_3 multilayers, Phys. Chem. Chem. Phys. 12 (2010) 14596–14608.
[32] C. Korte, A. Peters, J. Janek, D. Hesse, N. Zakharov, Ionic conductivity and activation energy for oxygen ion transport in superlattices—the semicoherent multilayer system YSZ (ZrO_2 + 9.5 mol% Y_2O_3)/Y_2O_3, Phys. Chem. Chem. Phys. 10 (2008) 4623–4635.
[33] R. Sanghavi, R. Devanathan, M.I. Nandasiri, S. Kuchibhatla, L. Kovarik, S. Thevuthasan, S. Prasad, Integrated experimental and modeling study of the ionic conductivity of samaria-doped ceria thin film, Solid State Ion. 204 (2011) 13–19.
[34] J.H. Hwang, D.S. McLachlan, T.O. Mason, Brick layer model analysis of nanoscale-to-microscale cerium dioxide, J. Electroceram 3 (1999) 7–16.
[35] N.J. Kidner, N.H. Perry, T.O. Mason, E.J. Garboczi, The brick layer model revisited: introducing the nano-grain composite mode, J. Am. Ceram. Soc. 91 (2008) 1733–1746.
[36] A. Tschope, Interface defect chemistry and effective conductivity in polycrystalline cerium oxide, J. Electroceramics 14 (2005) 5–23.
[37] S. Kim, J. Maier, On the conductivity mechanism of nanocrystalline ceria, J. Electrochemics. Soc. 149 (2002) J73–J83.
[38] D. Perez-Coll, P. Nunez, J.R. Frade, Improved conductivity of $Ce_{1-x}Sm_xO_{2-\delta}$ ceramics with submicrometer grain sizes, J. Electrochemics. Soc. 153 (2006) A478–A483.
[39] Z. Gao, X. Liu, B. Bergman, Z. Zhao, Comparative study of $Ce_{0.85}Sm_{0.075}Nd_{0.075}O_{2-\delta}$ electrolyte synthesized by different routes, J. Alloy Compd. 509 (2011) 8720–8727.
[40] J. Maier, Nanoionics: ion transport and electrochemical storage in confined systems, Nat. Mater 4 (2005) 805–815.